www.ijprems.com
editor@ijprems.com

INTERNATIONAL JOURNAL OF PROGRESSIVE RESEARCH IN ENGINEERING MANAGEMENT AND SCIENCE (IJPREMS)
(Int Peer Reviewed Journal)
Vol. 05, Issue 10, October 2025, pp : 700-706

e-ISSN : 2583-1062
Impact Factor : 7.001

IMPACT OF NITROGEN DOPING ON ZNO NANOPARTICLES OPTICAL, ELECTRICAL AND STRUCTURAL CHARACTERISTICS

Dr. Dipak A. Zope[1]

[1]Asst. Prof. Vidnyan Mahavidyalaya, Malkapu Dist Buldhana, India.

E-Mail ID: dipakaz14@gmail.com

ABSTRACT

This study investigates the impact of nitrogen doping on the structural, optical, and electrical properties of zinc oxide (ZnO) nanoparticles synthesized via a chemical precipitation method. Nitrogen-doped ZnO (N:ZnO) nanoparticles were prepared with varying dopant concentrations (0.5%, 1%, and 5%) and thoroughly characterized using XRD, TEM, UV–Vis spectroscopy, Raman, FTIR, and photoluminescence techniques. XRD analysis confirmed the retention of the hexagonal wurtzite structure across all samples, with minor lattice distortions and crystallite size increases observed upon nitrogen incorporation, particularly beyond 1% doping. TEM and EDAX analysis verified uniform particle morphology and successful nitrogen integration. UV–visible diffuse reflectance spectroscopy revealed a slight blue shift in the optical band gap, attributed to nitrogen-induced defect states and size-dependent quantum confinement effects. Raman and FTIR spectra showed evidence of structural modifications and nitrogen-related vibrational modes. Electrical measurements indicated doping-dependent variations in resistance and capacitance. Overall, nitrogen doping effectively modulates the nanostructural, optical, and electronic characteristics of ZnO, highlighting its potential in tuning material properties for optoelectronic applications.

Keywords: Nitrogen-Doped Zno, Nanoparticles, Optical Properties, Structural Analysis, Band Gap Engineering, Chemical Precipitation Method.

1. INTRODUCTION

Several wide band gap semiconducting materials have been investigated recently due to the demand for blue and UV solid-state emitters and detectors.[1-3]

Zinc oxide is regarded as a promising choice for optoelectronic devices such as photo detectors, ultraviolet laser diodes, and visible light emitting diodes because of its substantial exciton binding energy (60 meV) and direct band gap (3.2 eV).[2,3] Doping determines a wide range of ZnO's characteristics, which include high transparency, piezoelectricity, wide-band gap semi conductivity, room temperature ferromagnetism, a wide range of conductivity from metallic to insulating (including n-type and p-type conductivity), and significant magneto-optic and chemical sensing effects.[3]Near band-edge UV emission and deep-level emission are typically included in ZnO photoluminescence; the latter is associated with impurities and structural flaws.[2,3]

ZnO's broad band gap makes it transparent in the visible portion of the electromagnetic spectrum, which makes it useful for a variety of applications, including organic light-emitting diodes (OLED), transparent thin-film transistors (TTFT), shielding against high-energy radiation, blue/UV solid-state emitters[3], and transparent conducting oxides[4]. One significant benefit is that ZnO synthesis is less expensive than that of several other alternative semiconductors, including III-V semiconductors[6].

According to theoretical studies, a variety of doping mechanisms, including the substitution of Group-I elements (Li, Na) on a Zn site[7,8], large-size Group-V elements As or Sb on a zinc site [9], or Group-V elements on the O site[10], can result in shallow acceptor levels in ZnO.N impurities (deposited on the anion site) seemed to be creating shallow p-type dopants in semiconducting materials, and significant chemical trends in the energy levels of sp3-bonded substitution deep impurities in the wurtzite semiconductors were also anticipated.[10]

Therefore, the challenges encountered in identifying the appropriate dopant and growth procedures that lead to p-type conductivity and, subsequently, in the manufacture of a p-type ZnO material, either in the form of thin films or bulk crystal, limit its potential applications.

Motivated by the aforementioned reasons, our goal is to comprehend how nitrogen doping affects the optical and structural characteristics of ZnO nanoparticles. A facile chemical precipitation approach was adopted to prepare Nitrogen doped ZnO (N:ZnO) nanoparticles with varied dopant concentrations. The prepared samples underwent a number of characterizations, and the resulting outcomes were methodically examined.

The sintering temperature is a critical parameter for enhancing the crystalline quality of ZnO, as it significantly influences intrinsic defect populations and overall material properties. As the sintering temperature increases, recrystallization becomes more pronounced, leading to alterations in defect densities and grain structure.

www.ijprems.com
editor@ijprems.com

INTERNATIONAL JOURNAL OF PROGRESSIVE RESEARCH IN ENGINEERING MANAGEMENT AND SCIENCE (IJPREMS)
(Int Peer Reviewed Journal)
Vol. 05, Issue 10, October 2025, pp : 700-706

e-ISSN : 2583-1062
Impact Factor : 7.001

Consequently, variations in sintering temperature enable control over the concentration of defects such as oxygen vacancies and interstitial zinc—and allow tuning of the sample's structural, electrical, and optical characteristics

The electrical behavior of ZnO-based devices is strongly influenced by both grain size and the characteristics of grain boundaries. In particular, current–voltage responses predominantly arise from grain boundary effects, as the number of boundaries between electrodes largely dictates the nonlinear conduction and breakdown voltage of ZnO ceramics. Various optical properties of ZnO have been explored using multiple spectroscopic and imaging methods, including absorption, transmission, reflection, photoreflectance, spectroscopic ellipsometry, photoluminescence, cathodoluminescence, among others. In the present photoluminescence study, emission spans from the near-band-edge ultraviolet region to visible green or orange wavelengths, with a broad luminescence band centered around ~2.45 eV.

2. EXPERIMENTAL DETAILS

2.1 Sample preparation

To prepare nitrogen-doped ZnO nanoparticles, a chemical precipitation method was employed [11–12].All reagents were of analytical reagent (AR) grade. Separate aqueous solutions of zinc acetate dihydrate, monoethanolamine (MEA), and isopropyl alcohol (IPA) were prepared in doubly deionized (DI) water at 0.4 M concentration. To ensure thorough mixing, MEA and IPA solutions were gradually introduced dropwise into the zinc acetate solution under stirring. The resulting homogenous mixture yielded undopedZnO nanoparticles upon subsequent processing. In this precipitation approach, the solvent composition was carefully adjusted to induce the formation of ZnO nanoparticles by reducing their solubility compared to the surrounding solution[13–14].

To prepare N-doped ZnO (N:ZnO) nanoparticles with varied nitrogen levels—specifically 0.5%, 1% and 5% appropriate volumes of a 0.4 M aqueous ammonium acetate solution were introduced into the previously prepared mixture. The addition was carried out under continuous, gentle magnetic stirring, which is essential for effective precipitation of N:ZnO nanoparticles. The precipitate was then thoroughly rinsed with deionized water and dried at 200 °C for 8 h in an oven. The resulting powders include the undopedZnO and N:ZnO variants, labeled as 4MN05, 4MN10, 4MN50, and 4MN100, corresponding to the 0.5%, 1% and 5% nitrogen doping levels, respectively.

Research underscores that in chemical precipitation methods for ZnO synthesis, parameters such as pH, temperature, reactant concentration, and reagent addition rates critically influence the nucleation and growth pathways of nanoparticles ultimately controlling morphology, size, and crystallinity .

In situ investigations demonstrate that ZnO formation often proceeds via two distinct mechanisms dissolution reprecipitation and direct crystallization through dehydration and internal restructuring of precursor phases like $Zn(OH)_2$. Moreover, advanced studies reveal that nanoparticle evolution may involve both oriented attachment and Ostwald ripening, with the balance between these mechanisms depending on reaction kinetics and solution stability[13-15].In our synthesis, the deliberate slow addition of reactants is expected to enhance nucleation while suppressing subsequent growth of ZnO nanoparticles.

ZnO discs were fabricated using a conventional ceramic processing route, which encompassed ball milling, drying, pressing, and sintering steps. High-purity oxide powders (99.9%) with a composition of 99 mol% 20 nm ZnO and 0.5 mol% each of Bi_2O_3 and Mn_2O_3 were used as starting materials. The powders were mixed with polyvinyl alcohol (PVA) in distilled water and subjected to ball milling for 6 hours. The resultant ZnO slurry was dried in air at 60 °C for 1 hour, then sieved through a 20-mesh screen to produce granules. These granules were pressed into discs (26 mm in diameter, 2 mm thick) under a pressure of 4 ton/cm². The green bodies were finally sintered in air, at temperatures ranging from 980 °C to 1380 °C, each held for 3 hours.

2.2. Characterization

To investigate the structural, electronic, and optical properties, powder samples of undopedZnO and N-doped ZnO with doping levels of 0.5%, 1% and 5% were characterized using various analytical techniques. The crystalline phase and related parameters were examined through X-ray diffraction (XRD) using a Bruker D8 Advance diffractometer equipped with a Cu anode, producing Kα radiation of wavelength 1.544 Å, operated at 40 kV and 40 mA. The θ–2θ diffraction patterns of all samples were recorded at a scan rate of 3°/min. High-resolution transmission electron microscopy (HRTEM) images were obtained using a JEOL JEM-2100F microscope operating at 200 kV to analyze fine structural features. The same instrument was also employed for EDAX analysis to quantitatively estimate the chemical composition. Micro-Raman spectra were recorded using a RenishawInVia Raman microscope with an Ar^+ laser (514.5 nm wavelength, 50 mW) over the scanning range of 100–800 cm^{-1}. Infrared-active vibrational modes were studied using a PerkinElmer BXII FTIR spectrophotometer in the frequency range of 400–4000 cm^{-1}, with samples embedded in a KBr matrix and measured in transmittance mode. Room-temperature UV–visible reflectance spectra were collected in the wavelength range of 250–800 nm using a Perkin-Elmer Lambda-35 spectrophotometer.

www.ijprems.com
editor@ijprems.com

INTERNATIONAL JOURNAL OF PROGRESSIVE RESEARCH IN ENGINEERING MANAGEMENT AND SCIENCE (IJPREMS)
(Int Peer Reviewed Journal)
Vol. 05, Issue 10, October 2025, pp : 700-706

e-ISSN : 2583-1062
Impact Factor : 7.001

Microstructural observation of the ZnO discs was performed using a JEOL JSM-6460 LV scanning electron microscope equipped with energy-dispersive X-ray spectroscopy (EDX), while their phase composition was examined by high-resolution X-ray diffraction on a (PANalyticalX'Pert PRO MED PW3040) instrument, employing Cu Kα radiation (λ = 1.5406 Å).

2.3 Electrical and optical testing

The electrical characteristics of the samples were investigated using a high-voltage source-measure unit (Keithley 246). From the current–voltage (I–V) data, electrical resistance (RRR) was determined in accordance with Ohm's law. Capacitance and its frequency dependence were measured using an Impedance Analyzer. Room-temperature photoluminescence (PL) spectra were acquired on a JobinYvon HR-800 UV spectrometer. For structural analysis, Raman spectroscopy was performed using a LabRAM-HR system equipped with a 514.5 nm argon-ion laser.

3. RESULTS AND DISCUSSION

Powder X-ray diffraction (θ–2θ, 30–70°) for undoped and N-doped ZnO (0.5, 1and 5%) shows intense reflections at ~31.6°, 34.3°, 36.1°, 47.4°, 56.4°, 62.7°, 66.2°, 67.8°, and 68.9°, indexed to the (100), (002), (101), (102), (110), (103), (200), (112), and (201) planes of the hexagonal wurtzite structure. These peak positions and assignments match the standard ZnO reference pattern (ICDD/JCPDS 36-1451), confirming phase-pure wurtziteZnO across all compositions[13–14]

No additional reflections attributable to nitrogen-containing secondary phases are detected within the instrument's resolution, indicating that N incorporation does not produce crystalline impurity phases under the present processing conditions. Similar observations are widely reported for N-doped ZnO, where XRD typically reveals single-phase wurtzite with, at most, subtle peak shifts.

Peak positions provide insight into lattice strain. According to Bragg's law ($n\lambda = 2d \sin\theta$), an increase in interplanar spacing (lattice expansion) shifts peaks to lower 2θ, whereas a decrease (lattice contraction) shifts them to higher 2θ. In our data, the (101) reflection shows no discernible shift for 0.5% N relative to undopedZnO, but progressive, small shifts appear from ≥1% N, consistent with a modest strain state induced by N incorporation.[16]

The direction and magnitude of these shifts are consistent with partial substitution of O^{2-} by the slightly larger N^{3-} (Shannon radii), which can produce tensile strain and a corresponding downshift in 2θ, although the exact coordination-dependent radii and defect chemistry must be considered.

Peak broadening varies slightly with N content. Such broadening commonly reflects a combination of finite crystallite size and microstrain; if desired, crystallite sizes may be estimated via the Scherrer equation and size/strain contributions separated using Williamson–Hall analysis.[9,17,18]

Overall, the diffraction results demonstrate that all samples retain the wurtziteZnO crystal structure without detectable secondary phases, while nitrogen addition above ~1% introduces measurable lattice strain manifested as subtle (101) peak shifts and minor breadth changes. This behavior aligns with prior reports of single-phase N:ZnO exhibiting small, doping-dependent shifts in the principal ZnO reflections.[16]

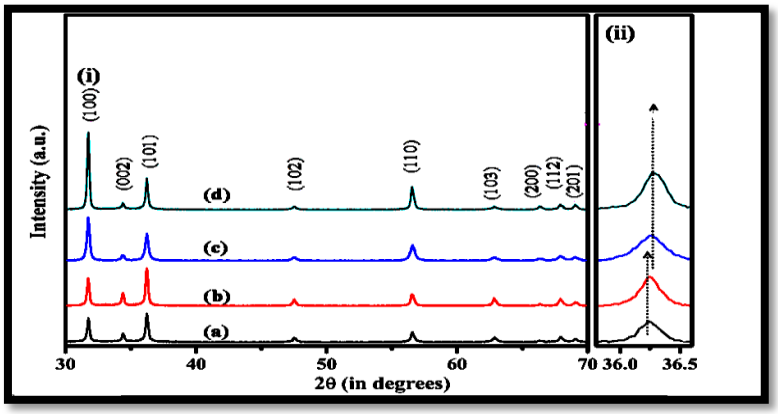

Fig 1: (i) XRD patterns of ZnO nanostructures: (a) undopedZnO; (b) 0.5% N:ZnO; (c) 1% N:ZnO; (d) 5% N:ZnO; (ii) Enlarged view of the (101) diffraction peaks, illustrating shifts in peak position and variations in peak broadening across the different samples.

Our XRD analysis reveals that nitrogen incorporation into the ZnO lattice is manifested by a shift in the (101) diffraction peak toward higher angles, indicating induced tensile strain. However, beyond a 1% N doping concentration, further lattice expansion appears to plateau suggesting that additional nitrogen incorporation does not

www.ijprems.com
editor@ijprems.com

INTERNATIONAL JOURNAL OF PROGRESSIVE RESEARCH IN ENGINEERING MANAGEMENT AND SCIENCE (IJPREMS)
(Int Peer Reviewed Journal)
Vol. 05, Issue 10, October 2025, pp : 700-706

e-ISSN : 2583-1062
Impact Factor : 7.001

further alter lattice parameters. Concurrently, notable changes in peak broadening are observed alongside the peak shift, implying modifications in crystallite size or internal strain.

These findings align with reports in the literature: nitrogen substitution is known to cause detectable strain in ZnO, as evidenced by similar XRD shifts and broadening behavior in related studies. Furthermore, the observed stabilization in lattice distortion beyond low doping levels corroborates the notion that the host lattice may accommodate limited dopant concentrations before saturating structural deformation effects. Finally, the correlation between peak broadening and crystallite size alteration is well documented in ZnO systems, often attributed to the combined effects of reduced grain size and increased microstrain.

To quantify our earlier qualitative observations, we calculated both the lattice parameters and the crystallite sizes of the samples. The lattice constants a, b, and c were computed using the standard formula for hexagonal systems, which relates the interplanar spacing to the crystal structure. Crystallite sizes (τ) were estimated using the Debye–Scherrer equation:

$$\tau = \frac{K\lambda}{\beta \cos\theta}$$

WhereK is the shape factor, λ is the X-ray wavelength, β is the full width at half maximum (FWHM) of a diffraction peak after correcting for instrumental broadening, and θ is the Bragg angle. The resulting numerical values are compiled in Table 1.

Table 1 shows that the lattice constants for 0.5% N-doped ZnO remain unchanged compared to undopedZnO. Beyond this doping level, beginning at 1% nitrogen, a measurable alteration in lattice constants emerges, which then remains essentially stable for higher doping levels. This quantitative behavior aligns with earlier qualitative observations. Additionally, Table 1 underscores the formation of nanometric crystallites across all samples. Notably, crystallite size increases even at the 0.5% N doping level, despite the absence of changes in lattice constants. As nitrogen possesses a larger ionic radius than oxygen, its incorporation likely facilitates this enlargement. However, similar to the lattice constants, the crystallite size plateaus beyond 1% N doping. Taken together, these results confirm that nitrogen doping induces structural modifications up to approximately 1%, after which further doping does not significantly affect crystal parameters or crystallite dimensions.

To further analyze size, morphology, and chemical composition of both undoped and N-doped ZnO nanostructures, TEM and EDAX measurements were conducted.

3.1 TEM and EDAX analysis

To validate our earlier qualitative observations, transmission electron microscopy (TEM) combined with energy-dispersive X-ray (EDX/EDAX) spectroscopy was utilized to assess the morphology and elemental composition of both undoped and N-doped ZnO samples. The TEM micrographs, shown in Figure 2, reveal the detailed nanostructured morphology across doping levels from 0.5% to 10%. High-resolution TEM (HR-TEM) images display well-defined lattice fringes, confirming the high crystallinity and uniformity of the prepared nanostructures.

Table 1: Crystallite Parameters of undoped and N:ZnO Samples.

Crystal Parameters	Samples				
	Undoped	4MN05	4MN10	4MN50	4MN100
a = b (A^0)	3.2553	3.2553	3.2785	3.2785	3.2785
C (A^0)	5.210	5.210	5.240	5.235	5.235
τ (nm)	29.20	34.3	37.7	37.8	37.6

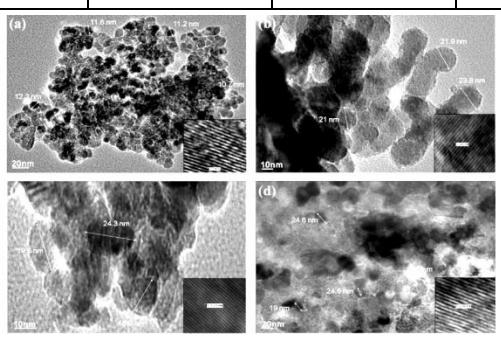

Fig 2: (a–d) TEM images of undoped and 0.5–10% N doped ZnO nanoparticles. Insets (a–d) HR-TEM images depicting the lattice fringes of respective samples.

www.ijprems.com
editor@ijprems.com

INTERNATIONAL JOURNAL OF PROGRESSIVE RESEARCH IN ENGINEERING MANAGEMENT AND SCIENCE (IJPREMS)
(Int Peer Reviewed Journal)
Vol. 05, Issue 10, October 2025, pp : 700-706

e-ISSN : 2583-1062
Impact Factor : 7.001

Table 2: Structural parameters determined through TEM images of undopes and N:ZnO Particles.

Structural parameters	Samples				
	Undoped	4MN05	4MN10	4MN50	4MN100
Particles Size Range (nm)	7-11	11-26	12-19	15-23	20-22
Model Particle (nm)	11	18	19	20	21
d-Spacing (nm) and Bragg Plane	0.163(110)	0.123(202)	0.260(002)	0.126(202)	0.145(103)

The HRTEM images (see insets in Figure 2) display clear lattice fringes, while Table 2 lists the corresponding interplanarspacings and associated crystallographic planes for both undoped and 0.5–5% N-doped ZnO nanostructures. These results confirm that all samples consist of nanocrystallineZnO, and that the fundamental lattice structure remains intact after nitrogen incorporation: each measured d-spacing corresponds to planes identified via XRD analysis. In terms of particle size, TEM-derived dimensions align well with those obtained from XRD, further validating the consistency of the data. Interestingly, the modal particle size increases in N-doped samples compared to the undoped ones. Indeed, a subtle increase in the modal nanoparticle size is observed, which supports the successful incorporation of nitrogen into the ZnO lattice.

3.2 UV–visible analysis

When particle sizes are too large for stable colloidal suspensions, optical absorption spectra become challenging to measure accurately, especially for precipitate-form samples. Since our undoped and N-doped ZnO nanoparticles were synthesized via a chemical precipitation route and collected as powders, diffuse reflectance spectroscopy (DRS) is the preferred method to probe electronic absorption. DRS overcomes the limitations of transmission-based measurements in scattering media by capturing reflectance from granular samples and enabling band-gap and electronic transition analysis from the remission spectrum.[19]

For band-gap evaluation via diffuse reflectance spectroscopy (DRS), the Kubelka–Munk formalism was applied using the K–M remission function. This approach is grounded in a continuum model in which light propagation through a diffusely scattering medium is described by two opposing radiant fluxes: one traveling downward and the other upward. These fluxes are each altered by absorption and scattering as they pass through infinitesimally thin layers, with changes in downward intensity partly compensated by upward-scattered radiation, and vice versa[16,20]

In the limiting case of an infinitely thick sample, the thickness and sample holder have no influence on the value of reflectance (R). In this case, the K–M equation becomessemiconductor, are related through equation as follows[20,21].

$$\frac{K}{S} = \frac{(1 - R_\infty)}{2R_\infty} = F(R_\infty) \dots\dots\dots\dots\dots\dots\dots\dots (2)$$

$F(R_\infty)$is the so called remission or KubelkaMumk Function. Wgere$R_\infty = R_{samples}R_{Standards}$ For parabolic band structure the band gap (E^g) and Absorption coefficient α of a direct band gapSemiconductor,are related through equation as follows[40,41]

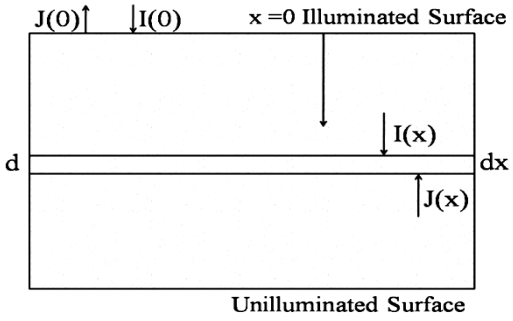

Fig 3: Model For the Kubelka-Munl analysis

$$\alpha h\nu = C_1(h\nu - E_g)$$

Where α is the linear absorption coefficient of the material, hν is the photon energy and C_1 is a proportionality constant.

When the material scatters in perfectly diffuse manner (or when its illuminated at 60^0 incidence), the K-M absorption coefficient K becomes equal to 2α (K = 2α). In this situation, Considering the K-M scattering coefficient S as Constant with respect to wavelength and using the remission function in Equation (3)

www.ijprems.com
editor@ijprems.com

INTERNATIONAL JOURNAL OF PROGRESSIVE RESEARCH IN ENGINEERING MANAGEMENT AND SCIENCE (IJPREMS)
(Int Peer Reviewed Journal)
Vol. 05, Issue 10, October 2025, pp : 700-706

e-ISSN : 2583-1062
Impact Factor : 7.001

We can obtain the expression

$$[F(R_\infty)hv]^2 = C_2(hv - E_g) \dots\dots\dots\dots\dots\dots\dots (4)$$

Therefore obtaining$F(R_\infty)$ from equ. (2) and plotting the $[F(R_\infty)hv]^2$against hv the band gap E_g of a powder sample can be extracted[16]

The Kubelka–Munk (K–M) model assumes that diffuse reflectance arises from the combined effects of light absorption and scattering at the surface. Given that our undoped and N-doped ZnO samples are nanopowderwhere the high surface-to-volume ratio enhances scattering applying the K–M approach is particularly appropriate for analyzing their optical absorption and band-gap characteristics.[16]

The room-temperature UV–visible diffuse reflectance spectra of both undoped and N-doped ZnO nanoparticles (0.5%, 1% and 5%) were acquired across the 250–850 nm range, as displayed in Figure 5(a–e). From the Kubelka–Munk transformed reflectance data, the estimated optical band gap of the nanoparticles is approximately 3.3 eVa noticeable blue shift compared to the bulk ZnO band gap of around 3.37 eV. This upward shift in energy is attributed to quantum size confinement effects inherent to the nanoscale, where reduced particle dimensions increase the band gap.[13]

The modest blue shift of approximately 0.1 eV in the band gap of N-doped ZnO, compared to undopedZnO, suggests that the effect arises primarily from the introduction of nitrogen-related defect states rather than strong quantum confinement consistent with the relatively large particle sizes observed via XRD and TEM. Since N-doped nanoparticles are larger, the shift is unlikely due to size reduction; instead, nitrogen introduces shallow electronic states near the valence or conduction bands that marginally raise the optical transition energy. This behavior aligns with the known role of dopants in semiconductors, where the formation of impurity levels adjacent to band edges can influence absorption characteristics [21].

Recent studies indicate that nitrogen can substitute for oxygen in ZnO to form NO acceptor sites. When these N_o centers pair with zinc vacancies (V_Zn), they may behave as shallow acceptors; moreover, hydrogen can further stabilize these complexes, reducing their ionization energy and facilitating p-type behavior. First-principles calculations show that the NO–V_Zn defect complex in the presence of hydrogen (forming V_Zn–NO–H) possesses significantly lower formation energy and exhibits shallow acceptor activity being a more viable contributor to conductivity than isolated NO sites. Additionally, hydrogen-mediated donor–acceptor pairing may shift extremely deep acceptor states closer to the valence band, further enhancing their electronic activity.[22,23]

As the Kubelka–Munk (K–M) model presumes that diffuse reflectance is generated by surface scattering and absorption, it is particularly suitable for nanopowders such as ZnO. In our study, both undoped and N-doped ZnO nanoparticles were prepared via chemical precipitation, resulting in a high surface-to-volume ratio exactly the condition where K–M theory excels for optical absorption analysis and band-gap determination.

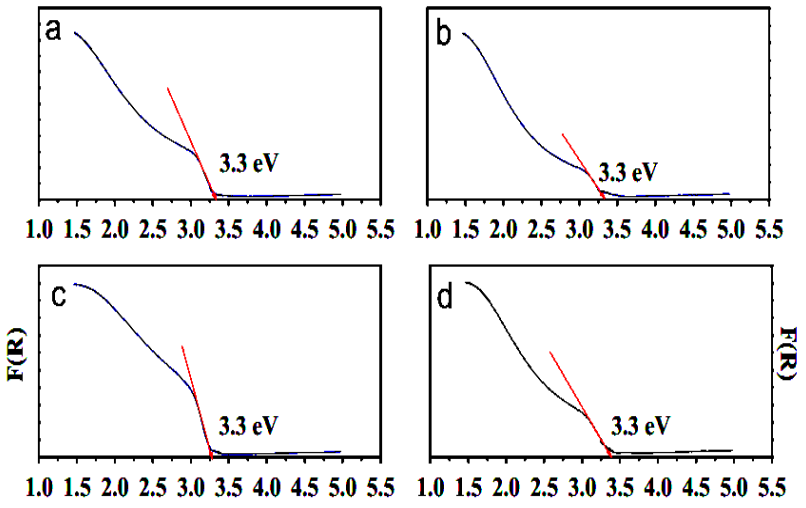

Fig 4: UV–visible reflectance spectra of (a) undopedZnO, (b) 0.5%, (c) 1%, (d) 5% nanoparticles.

For diluted semiconductors like ZnO:N, nitrogen-related defect levels are situated just above the valence band, enabling optical absorption transitions from these shallow acceptor states into higher conduction band levels. Figure 6 schematically illustrates the combined effects of nanoscale dimensions and nitrogen doping on the electronic structure of ZnO, and the associated optical absorption pathways.

The observed slight blue shift in the optical absorption edge can be attributed to the combined effects of nanoscale size and nitrogen-induced defect states within the electronic structure of ZnO. In our nanostructured samples, the increased

surface-to-volume ratio enhances the influence of discrete energy levels, while nitrogen doping introduces localized states that modify the band-edge absorption behavior[13,22,23]

The modal particle size of manufactured ZnO nanoparticles increases from 11 nm (for undoped) to 18–22 nm (for N doped) in line with XRD analysis, TEM, and EDAX research. The energy band gap has been seen to slightly move blue from 3.2 eV to 3.3 eV as a result of N doping. Furthermore, FTIR analysis confirms that the substitution of N for O in the ZnO lattice causes the NO–H mode to arise when N:ZnO is passivated by H.The quantitative decrease of Raman spectra peaks demonstrated the progressive weakening of fundamental ZnO modes in the presence of N impurity. Furthermore, the modifications in various IR and Raman vibrational modes seen along with the emergence, shifts and gradual prominence of N:ZnO modes, vividly demostrate the proportional incorporation of N in ZnO lattice for 0.5–5% N:ZnO nanostructures.

4. REFERENCES

[1] S.J. Henley, S. Silva, and M.R. Alenezi, Sci. Rep. 5 (2015) 8516.
[2] J. Phys. 16 (2004) R829, Z.L. Wang.
[3] J. Appl. Phys. 98 (2005) 041301; Ü. Özgür, Y.I. Alivov, C. Liu, A. Teke, M. Reshchikov, S. Doğan, V.Avrutin, S.J. Cho, and H. Morkoc.
[4] Thin Solid Films 442 (2003) 167–172; C. Agashe, O. Kluth, G. Schöpe, H. Siekmann, J. Hüpkes, B. Rech.
[5] Jpn. J. Appl. Phys. 44 (2005) L1193, J. Nishii, A. Ohtomo, K. Ohtani, H. Ohno, and M. Kawasaki.
[6] C.G. Van de Walle and A. Janotti, Phys. Rev. B 76 (2007) 165202.
[7] C. Park, Phys. Rev. B 66 (2002) 073202.
[8] Phys. Rev. B 70 (2004) 115210, E.C. Lee, K. Chang.
[9] S. Zhang, S.H. Wei, C. Park, S. Limpijumnong, Phys. Rev. Lett. 92 (2004) 155504.
[10] Phys. Rev. B 28 (1983) 946, A. Kobayashi, O.F. Sankey, and J.D. Dow.
[11] Goswami, N.; Sahai, A. Mater. Res. Bull. (2013) 346–351.
[12] Wang, L.; Muhammed, M. J. Mater. Chem. (1999) 2871–2878.
[13] Goswami, N.; Sharma, D. K. Physica E (2010) 1675–1682.
[14] Sahai, A.; Goswami, N. Ceram. Int. (2014) 14569–14578.
[15] Goswami, N.; Sahai, A. MRS Online Proceedings Library (2013) mrss13-1551-r1510-1515.
[16] Sahai, A.; Kumar, Y.; Agarwal, V.; Olive-Méndez, S.; Goswami, N. J. Appl. Phys. (2014) 164315.
[17] Z.B. Gu, M.H. Lu, J. Wang, D. Wu, S.T. Zhang, X.K. Meng, Y.Y. Zhu, S.N. Zhu, Y.F. Chen, X.Q. Pan, Appl. Phys. Lett. 88 (2006) 082111.
[18] M. Dutta, T. Ghosh, D. Basak, J. Electron. Mater. 38 (2009) 2335–2342.
[19] D.G. Barton, M. Shtein, R.D. Wilson, S.L. Soled, E. Iglesia, J. Phys.Chem. B 103 (1999) 630–640.
[20] P. Kubelka, F. Munk, Z. Tech. Phys 12 (1931) 593–599
[21] J.I. Pankove, Courier Corporation, 2012.
[22] A. Boonchun, W.R. Lambrecht, Phys. Status Solidi B 250 (2013)2091–2101.
[23] S. Lautenschlaeger, M. Hofmann, S. Eisermann, G. Haas, M. Pinnisch,A. Laufer, B. Meyer, Phys. Status Solidi B 248 (2011) 1217–1221.